Enhanced interfacial wettability and mechanical properties of $Ni@Al_2O_3/Cu$ ceramic matrix composites using spark plasma sintering of Ni coated Al_2O_3 powders

Tao Feng[a], Wei Zheng[a], Wenge Chen[a*], Yingge Shi[a], Yong Qing Fu[b*]

[a] School of Materials Science and Engineering, Xi'an University of Technology, Xi'an, Shaanxi, 710048, P.R. China

[b] Faculty of Engineering and Environment, Northumbria University, Newcastle upon Tyne, NE1 8ST, UK.

Abstract: Poor wettability and weak interfacial bonding between Cu and Al_2O_3 have been critical issues for sintering of high-quality $Ni@Al_2O_3/Cu$ composites. In this paper, we explore an interfacial engineering design methodology to achieve good mechanical properties of $Ni@Al_2O_3/Cu$ composites using spark plasma sintering method. The Ni coated powders were prepared using a heterogeneous precipitation method, which can significantly improve wettability between Cu and Al_2O_3 and enhance their interfacial bonding. The sintered $Ni@Al_2O_3/Cu$ composites with a copper content of 15 vol% showed a compact network structure of alumina well-infiltrated with metallic Cu, and achieved good mechanical (e.g., fracture toughness of 6.72 $MPam^{1/2}$) and physical properties (e.g., relative density of 99.3% and electrical resistivity of 1.2810^{-3} Ω.m). The key mechanisms for the enhanced properties of the composites synthesized using the Ni coated composite powders have been identified as: (1) well-formed ceramic/metal interfacial structures which improve

* Corresponding author: Professor Wenge Chen

E-mail: wgchen001@263.net (Wenge Chen), richard.fu@northumbria.ac.uk (Richard Yongqing Fu)

wettability of Al_2O_3 with Cu, and promote the formation of a homogeneous network structure; (2) enhanced elemental diffusion and interfacial reactions, which result in formation of Cu_2O and $CuAlO_2$ and thus improve interfacial wetting and bonding properties.

Key words: Heterogeneous precipitation; Ni@Al_2O_3/Cu composites; composite powders; Interfacial structure

1. Introduction

Alumina (Al_2O_3) exhibits good characteristics of high melting point, high elastic modulus, high hardness and good chemical stability, but its low fracture toughness and poor thermal conductivity have seriously limited its wide-range engineering applications [1–4]. Whereas a metal such as copper has excellent electrical and thermal conductivities, but has low yield strength/hardness and poor wear resistance. Introduction of a network structure of ductile metal into a ceramic (alumina) matrix not only improves sinter-ability, electrical and thermal conductivities of the composite, but also maintain high strength, toughness and ductility [5–7]. However, the wettability and interfacial bonding between copper and alumina are always critical issues. It was reported that [8] the wetting angle of the copper on alumina substrate was 128°under a vacuum at 1200^{o}C. The poor wettability results in a poor interfacial strength and an uneven distribution of the Cu phase within ceramic matrix during sintering, thus the properties of the sintered composites are not as good as expected. Therefore, it is critical to find new methods to prepare Ni@Al_2O_3/Cu composites with uniform composition/microstructures and improve their physical and mechanical properties for their potentially wide-range applications.

In order to solve the problem of poor wettability between metal and ceramic, one commonly applied method is to coat the surfaces of ceramic particles with a layer of metal and form composite powders with a core-shell structure [9–13]. This type of interfacial engineering method has been applied in literature. For example, Beygi et al. [14] prepared Cu/Al_2O_3 composite powders using a chemical plating method and studied effects of different coating parameters on the properties of the composite powders. Lu et al. [15] prepared Cu coated Al_2O_3 powders using a hot-pressing method at 1500 ^oC and the fracture toughness of the composite material has been significantly improved. Uysal et al. [16] synthesized Ni coated Al_2O_3 powders using an electroless plating method and found that the Ni coating was adhered well to the ceramic substrate. Mazaher et al. [17] synthesized TiB_2 coated B_4C powders which were incorporated into aluminum matrix, and found that the wear resistance of the composite was considerably higher than that of the matrix alloy.

In order to form Al_2O_3 framework structure in the composite, the sintering temperature of the composite material is generally high, and often exceeds the melting point of metallic Cu. Therefore, although the Cu coated alumina powders have been often used, the covered copper layers will be easily melted during the sintering process. This will lose the Cu layers on the Al_2O_3 powder surfaces, and thus there are not many differences for the mechanical properties between the sintered products made using the conventionally mixed powders and those using the Cu coated ones. For this reason, researchers proposed to use metals with higher melting points such as Fe and Ni as the coating materials on the Al_2O_3 powder surfaces [18–19]. However,

Fe is easily oxidized at the high temperature, and has a poor corrosion resistance with less infiltration possibility compared with copper.

In this study, composite powders of Ni coated Al_2O_3 (e.g., Ni@Al_2O_3) were prepared using a heterogeneous precipitation method to form a good ceramic/metal interface and improve the wettability/bonding between alumina and copper. Our previous study reported [20] that spark plasma sintering (SPS) plays an important role in improving the homogeneity, density and physical mechanical properties of Ni@Al_2O_3/Cu composites during the sintering of Al_2O_3 and Cu powders. Therefore, in this study, SPS will be used to prepare Ni@Al_2O_3/Cu composites by sintering the Ni@Al_2O_3 composite powders and Cu powders. The Cu powders with a mixing ratio of 15 vol% was found to distribute homogenously inside the alumina matrix. Effects of Ni coating on microstructures, physical and mechanical properties as well as wettability and strengthening mechanisms of the composites were investigated systematically.

2. Experimental

2.1 Raw materials

Commercially available Al_2O_3 powders (with a purity of 99.4% and an average particle size of 1~3μm) and electrolytic copper powders (with a purity of 99% and an average particle size of about 4–6 μm) were purchased from Fuchen Chemical Reagent Co., Ltd, Tianjin, China. The detailed information of the chemicals is listed in Table 1. All the other chemicals were obtained from Sinopharm Chemical Reagent Co. Ltd., Shanghai, China.

Table 1. Chemical compositions of Al_2O_3 and Cu powders (mass fraction, %).

Powders	α-Al_2O_3	Cu	Fe	Cl	Pb	Mn
α-Al_2O_3(wt%)	≥99.4	-	0.01	0.01	0.005	＜0.005
Cu(wt%)	-	≥99	0.008	＜0.1	-	＜0.005

2.2 Synthesis of Ni@Al_2O_3 powders

The Ni@Al_2O_3 composite powders were prepared using a heterogeneous precipitation method by mixing Al_2O_3 particles inside the solutions of $NiSO_4·6H_2O$ and NH_4HCO_3. Firstly 150 mL of solution A of $NiSO_4·6H_2O$ with a concentration of 0.06 mol/L were prepared. Al_2O_3 of 5 g was added into the above solution A. In order to prevent the agglomeration of the Al_2O_3 powders, due to their small sizes, surfactant of polyethylene glycol (PEG) was added (Fig.1 (a)). Secondly, 150 mL of solution B with a concentration of 0.1 mol/L NH_4HCO_3 was prepared (Fig.1 (b)) and then slowly added into the solution A under a continuous stirring.

The pH value of the solution was controlled to be 8~9 during the reaction process. After a period of reaction at room temperature, the color of the solution was changed from pale green to dark green with the generation of a large amount of bubbles. After the reaction was completed without any bubble appeared, the precipitates were filtered, washed three times with deionized water and alcohol, and then dried to obtain the powders, There are alumina powders with their surfaces covered with $NiCO_3•2Ni(OH)_2•2H_2O$.Finally, the Ni@Al_2O_3 composite powders were obtained by annealing the above powders in a vacuum furnace at 580^oC for 2 hours in the H_2 atmosphere. The whole experimental process is illustrated in Fig. 1.

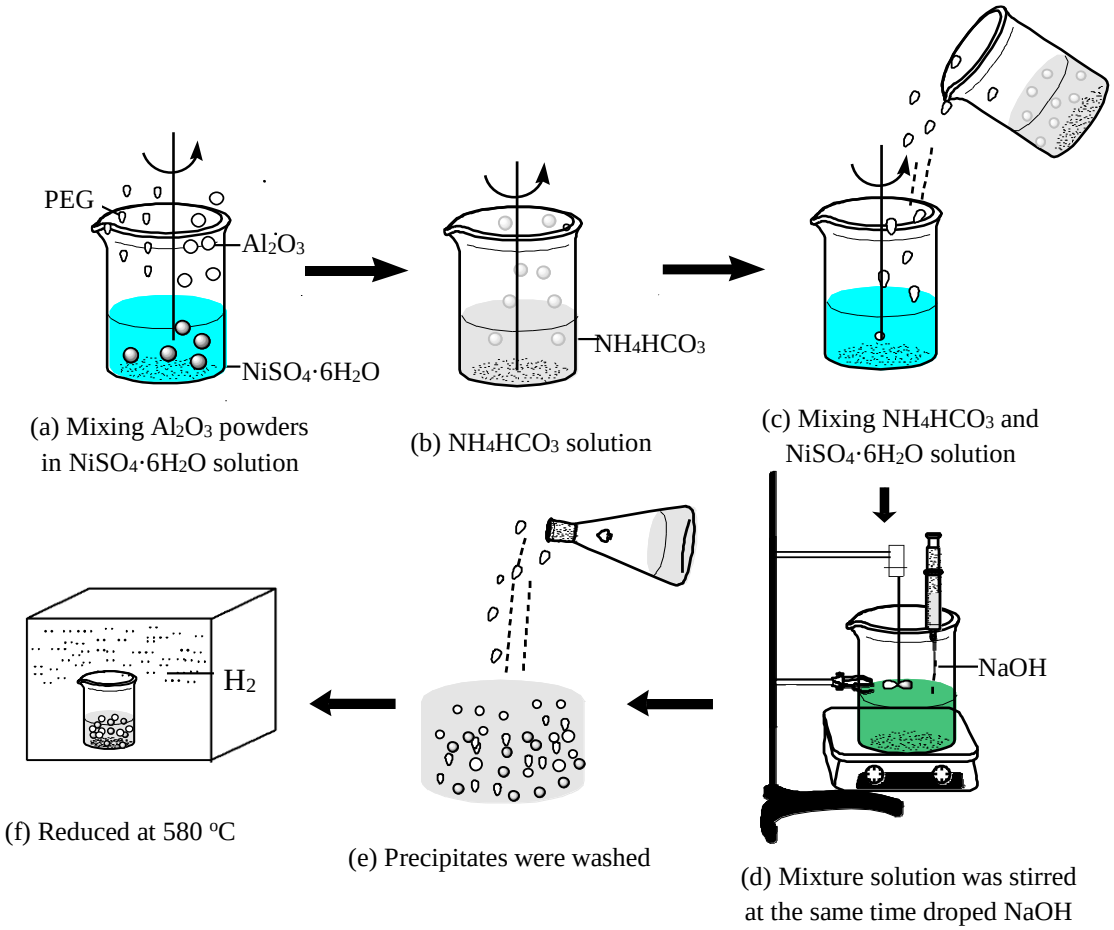

Fig. 1. Illustration of synthesis procedures of Ni@Al_2O_3 composite powder using a heterogeneous precipitation method.

2.3 Sintering of Ni@Al_2O_3/Cu composites

The Ni@Al_2O_3 composite powders were mixed with Cu powder (with a purity of 98% and average particle sizes of about 4–6 μm). The composites were ball-milled for 1 hour using stainless steel balls with diameters of 2 mm in a stainless steel container using a QMIF planetary ball milling machine (with a rotation speed of 40 revolutions per minute). Ar gas was used during the ball milling to reduce the oxidation of the Cu powder. The mixture was loaded in a graphite mold inside the SPS furnace (LABOX-330 SPS) with a vacuum of 1 Pa. Finally, the mixed powders were sintered

at 1350^{o}C with an initial heating rate of 50^{o}C/min, a pressure of 30 MPa and a dwell time of 10 min in an argon atmosphere.

2.4 Characterization

Morphology of Ni@Al_2O_3 powders, surface and fracture surface morphologies of the Ni@Al_2O_3/Cu composites were characterized using a scanning electron microscope (SEM, JSM-6700), attached with an energy dispersive X-ray spectrometer (EDX) for composition analysis. X-ray diffractometer (XRD, Rigaku, SmartLab, Japan, Cu Kα X-ray radiation; wavelength λ= 1.5418 Å) was used to analyze the crystalline structures of Ni@Al_2O_3 powder and the Ni@Al_2O_3/Cu composites. The scanning rate was 1°/min and the scanning range of 2θ was 20–80° with a step size of 0.01°. Interfacial structures of Cu-Ni-Al_2O_3 composites were characterized using a high-resolution transmission electron microscopy (HR-TEM, Talos F200X, FEI). The chemical binding states of chemical elements on the composite surfaces were characterized using X-ray photoelectron spectroscopy (XPS; PHI Quantera II, with Al Kα radiation source of 1486.4 eV) and Auger electron spectroscopy (PHI 4700 AES) at a vacuum of 4×10^{-8} Torr. In XPS analysis, the adventitious carbon cannot be used as a reliable binding energy reference, as this may cause an error in binding energy interpretation as large as ~2.66 eV due to variations in work functions of the tested samples [21,22]. Therefore, the calibration was performed by identifying the center position of metallic Cu peak from the Ni@Al_2O_3/Cu composite sample. This calibration method has been applied for calibration using the metallic manganese element (Mn) [23].

Contact angles of melt copper drop on alumina matrix were measured using an OCA20 contact angle analyzer at room temperature based on a droplet-based method reported in ref [24]. The specific operation procedures are as follows. Firstly, the copper billet was placed on an alumina substrate and sintered at a high temperature of 1350^{o}C. When the temperature was above the melting point of copper (1083^{o}C), the copper billet was melted and the Cu was spread on the alumina substrate. As the temperature was decreased during rapid cooling, the molten copper was condensed and formed an ellipsoid on the alumina substrate. The contact angle of solidified droplet on alumina was measured at the room temperature.

Hardness values of the composites were measured using a TUKON 2100 Vickers Microhardness Tester. Fracture toughness values of the Ni@Al_2O_3/Cu composites were obtained by measuring the lengths of cracks generated from a conventional indentation method on the composite surface using the Eq.(1):

$$K_{1C}=0.203H_V a^{\frac{1}{2}}\left(\frac{c}{a}\right)^{\frac{-3}{2}} \quad (1)$$

where K_{1C} is fracture toughness (MPa·$m^{1/2}$), Hv represents Vickers hardness (MPa), 2*a* is indentation diagonal length (mm), *c* is the half length of the indentation induced crack (mm).

3. Results and discussion

3.1 Microstructure and nucleation mechanism of Ni@Al_2O_3 composite powder

Fig. 2(a) shows the SEM images of pure Al_2O_3 powders, which exhibit smooth surfaces with an irregular morphology and an average particle size of about 1~3 μm.

Figure 2(b) shows the surface morphology of Ni@Al_2O_3 composite powders, whose surfaces are clearly coated with a layer of nanoparticles. The main chemical element of these nanoparticles is Ni, which can be identified from EDX analysis (see the attached Table in Fig. 2(b)).

Figure.2(c) shows XRD patterns of the Ni@Al_2O_3 composite powders. Comparing JCPDS card No. 04-0850, the diffraction angles 2θ at 44.50°, 51.85°, and 76.37° are corresponding to Ni's crystal plane indices of (111), (200), and (220), and the other peaks are belonged to those of Al_2O_3. Only the diffraction peaks of Al_2O_3 and Ni appear in the figure, and no other phases are detected, indicating that these small particles in Fig.(2b) is metal Ni, which confirms that the Ni coated Al_2O_3 composite powders were obtained after using the heterogeneous precipitation process. Ni grain size is estimated to be 35 nm according to the Scherrer's formula [25]. The result is consistent with that observed from the SEM analysis.

During the experimental process, as illustrated in Fig. 1(d), the reaction (2) will take place in the suspension.

$$3Ni^{2+}+6HCO_3^-+H_2O=NiCO_3\bullet 2Ni(OH)_2\bullet 2H_2O\downarrow+5CO_2\uparrow \quad (2)$$

There is a competition between homogeneous and heterogeneous precipitations or nucleation of $NiCO_3\bullet 2Ni(OH)_2\bullet 2H_2O$ on the Al_2O_3 from the solution. Based on the thermodynamics theory, the critical energies for homogeneous and heterogeneous nucleation of $NiCO_3\bullet 2Ni(OH)_2\bullet 2H_2O$ can be written in the Equations (3) and (4), respectively [26]:

$$\Delta G_c = \frac{16\pi\sigma^3}{3(\Delta G_v)^2} \quad (3)$$

$$\Delta G_c^* = \Delta G_c \left[\frac{(2+\cos\theta)(1-\cos\theta)^2}{4} \right] \quad (4)$$

where ΔG_c is the critical energy for homogeneous nucleation, ΔG_c^* is the critical energy for heterogeneous nucleation, σ is the liquid-solid boundary surface energy, ΔG_v is the change of free energy per unit volume, and θ is the contact angle of the generated nuclei on the matrix. Combining equations (3) and (4), when $0 \leq \theta \leq \pi$, the value of $\frac{(2+\cos\theta)(1-\cos\theta)^2}{4} \leq 1$, which means that the energy required for the heterogeneous nucleation, ΔG_c^*, is less than that for the homogeneous nucleation energy ΔG_c. Therefore, the formed $NiCO_3 \cdot 2Ni(OH)_2 \cdot 2H_2O$ tends to nucleate on the surface defects in order to reduce the surface energy, whereas the coarse surface of the alumina provides the favorable positions for the formation and accumulation of the nuclei. In the heating process (Fig.1(f)), $NiCO_3 \cdot 2Ni(OH)_2 \cdot 2H_2O$ was decomposed into NiO, and the NiO can react with H_2 based on the following reaction (5):

$$NiO + H_2 \rightarrow Ni + H_2O \qquad \Delta G^0 = -6916.7 - 37.12T \quad (5)$$

Finally, a layer of nickel is fully covered on the surface of the alumina. A schematic illustration of the nucleation of Ni layer is shown in Fig. 2(d).

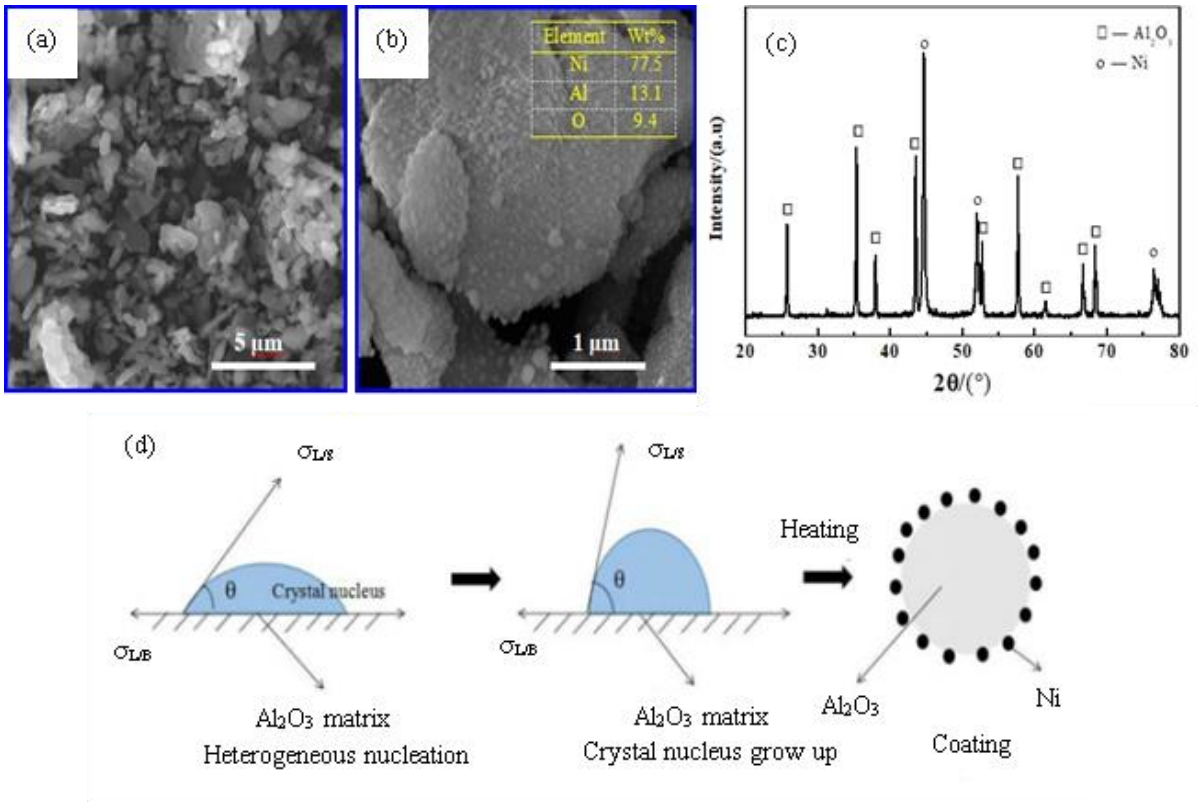

Fig.2.SEM images of (a)pure Al_2O_3 powders and (b)Ni@Al_2O_3 powders, (c)XRD patterns of Ni@Al_2O_3 composite powders, (d)Illustrations of nucleation mechanism of Ni@Al_2O_3 composite powders.

3.2 Microstructure and properties of Ni@Al_2O_3/Cu Composites

Fig. 3 shows the surface morphology and element mapping of Ni@Al_2O_3/Cu (15vol% Cu) composites after the SPS process. As the Ni and Cu have higher atomic numbers than that of Al in the alumina, the metal particles are white and the alumina ones are dark in the BSE image. The Cu phase are uniformly dispersed inside alumina with fine structures (as shown in Figs. 3(a) and 3(b)), which indicates that the molten metal is effectively infiltrated into the ceramic skeleton structures. From the high magnification SEM image shown in Fig. 3(c), we can see that the composite has a compact structure without apparent porosity.

In order to identify the phase distributions of ceramic and metal, EDX mapping performed, and the results are shown in Figs. 3(d) to 3(f). It can be confirmed that the Al_2O_3 forms a three-dimensional skeleton pattern and the metals (e.g. Ni and Cu) are uniformly distributed inside the composite, without apparent agglomeration of metal or ceramic phases. A small amount of Ni particles can be detected along with the Cu phase. Surface morphology study indicates that the Cu particles are mainly distributed at the grain boundaries of alumina and surrounded by the Ni particles, and the copper is well bonded onto the surface of the alumina matrix. In our previous study [20] of the composite without using any Ni layer, the molten copper can be infiltrated into the alumina skeleton due to the plastic flow and the high pressure during the SPS process. However, the infiltration was not well achieved and the distribution of the copper phase in the alumina was relatively inhomogeneous due to the poor wettability between the Cu phase and alumina. Therefore, for the composite synthesized using the SPS without Ni layer on the alumina, the sintering is more dependent on the large external forces without formation of effective bonding structures, thus the interfacial bonding of the composites is relatively poor.

However, after the Al_2O_3 powders were coated with the Ni layer though the interfacial engineering approach used in this study, the Ni and Cu were well-mixed during the sintering. The molten Cu was not directly bonded to the ceramic but instead bonded to the Ni layer on the alumina surface, which effectively improves the wettability and promotes the good bonding of interfaces. The molten copper could be easily and uniformly distributed around the metal Ni, which can be supported by the results

shown in Figs. 3(d)~3(f). Therefore, the Ni coated alumina improves the interfacial bonding between alumina and copper and also the uniformity of the microstructure through this interfacial engineering design, which will improve the mechanical properties of the composite.

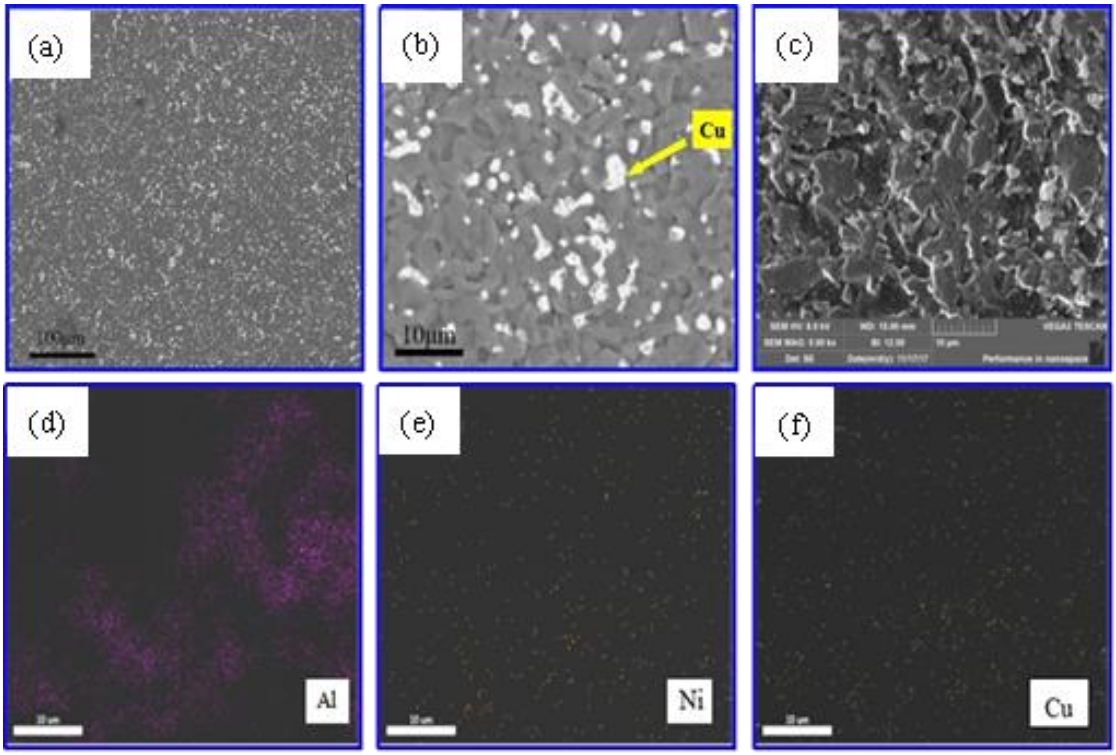

Fig. 3. Surface morphology and element mapping of Ni@Al_2O_3/Cu (15 vol% Cu) composites after SPS, (a) and (b) Backscattered electron (BSE) image, with low and high magnifications; (c) SEM image at a high magnification;(d) to (f) EDX Al element mapping, Ni element mapping and Cu element mapping.

Fig. 4 shows the fracture morphology of Ni@Al_2O_3/Cu composites, in which Fig. 4(a) is a low magnification image and Fig. 4(b) is a high magnification one. The fracture surface exhibits a quasi-cleavage fracture morphology. EDX line scanning results of elements on the cross-section surface of sample are shown in Fig. 4(c). Aluminum is consistently detected along the scanned line, indicating the continuity of the alumina

skeleton in the composite. Whereas those of line scanning results of Cu and Ni elements are not continuously observed. As can be seen from Fig. 4(c), the peak of Cu coincides with that of Ni. In addition, the uniform spacing of the peak indicates the uniform distribution of the metal in the alumina matrix, as illustrated in Fig. 4(d).

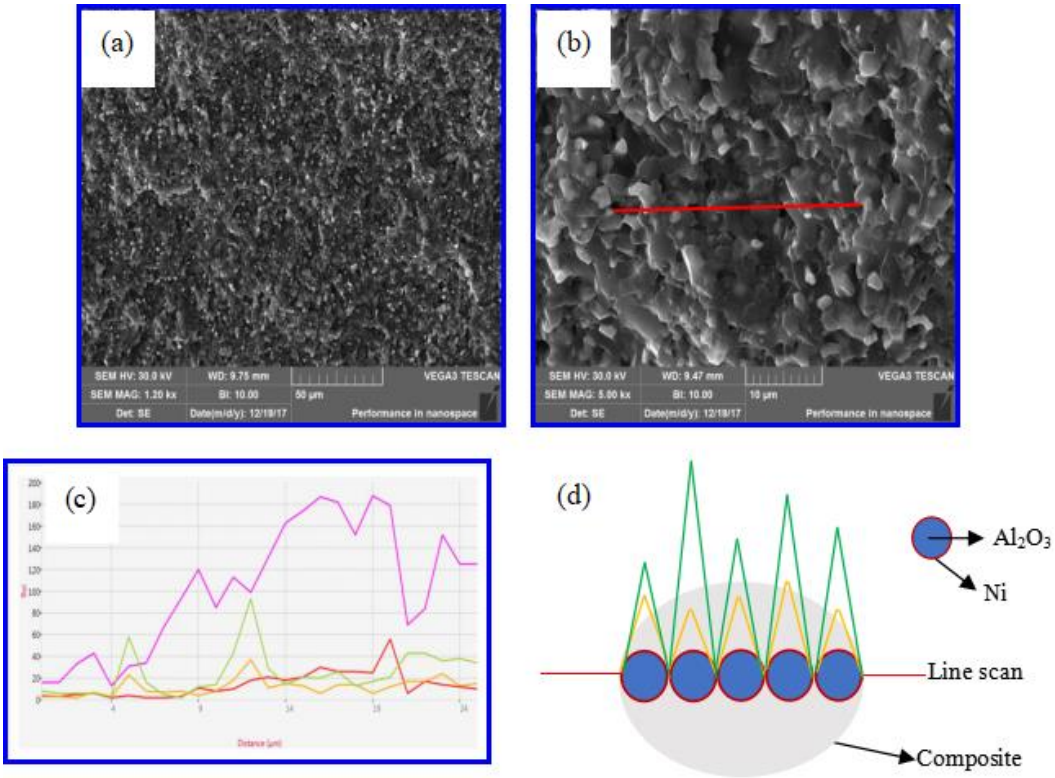

Fig. 4. (a) and (b): Low magnification and high magnification fracture morphologies of the Ni@Al_2O_3/Cu composites after Ni coating; (c) interfacial line scan spectra of the Ni@Al_2O_3/Cu;(d) schematic illustrations of composites line scan spectra.

Fig.5 shows XRD results of Ni@Al_2O_3/Cu composites after the SPS. The diffraction peaks of Al_2O_3 can be clearly seen from this figure, and the intensity of the Al_2O_3 peak is high, indicating its highly crystallized state. Comparing with the XRD patterns of Ni@Al_2O_3 composite powders (Fig.1(b)), those of Ni@Al_2O_3/Cu after the SPS do not show the diffraction peak of Ni, indicating that the Ni atoms are completely diffused into the Cu phase during sintering. Comparing the JCPDS card No. 04-0836,

we can conclude that the diffraction peak of Cu is slightly shifted to the right-hand side of the original position, mainly due to the lattice distortion of Cu due to the CuNi substitutional solid solution formation. In literature, the diffraction peaks of $CuAlO_2$ and Cu_2O can often be detected, indicating that during sintering the possible chemical reactions (6)~(9) occur[27-28]:

$$4Cu+O_2 \rightarrow 2Cu_2O \qquad \Delta G^0(J/mol) = -169702+74.12T \qquad (6)$$

$$2Cu_2O+O_2 \rightarrow 4CuO \qquad \Delta G^0(J/mol) = -62354+44.89T \qquad (7)$$

$$Cu_2O+Al_2O_3 \rightarrow 2CuAlO_2 \qquad \Delta G^0(J/mol) = -5670+2.49T \qquad (8)$$

$$CuO+Al_2O_3 \rightarrow CuAl_2O_4 \qquad \Delta G^0(J/mol) = 4403-4.97T \qquad (9)$$

All the Gibbs free energies (ΔG_0) of the above chemical reactions are negative at a sintering temperature of 1350 °C, indicating that all these chemical reactions can proceed spontaneously during sintering. Formation of these oxides and interfacial compounds (such as $CuAlO_2$) is beneficial for liquid sintering, thus enhancing the sintering kinetics due to their low melting points, e.g. CuO (1200^{o}C) and Cu_2O (1235 ^{o}C). However, in this study because the sintering was performed in an Ar atmosphere, there is a low partial pressure of oxygen[29], and CuO and $CuAl_2O_4$ might not be stable during the sintering. This might be the main reason that their diffraction peaks have not been detected from the XRD pattern.

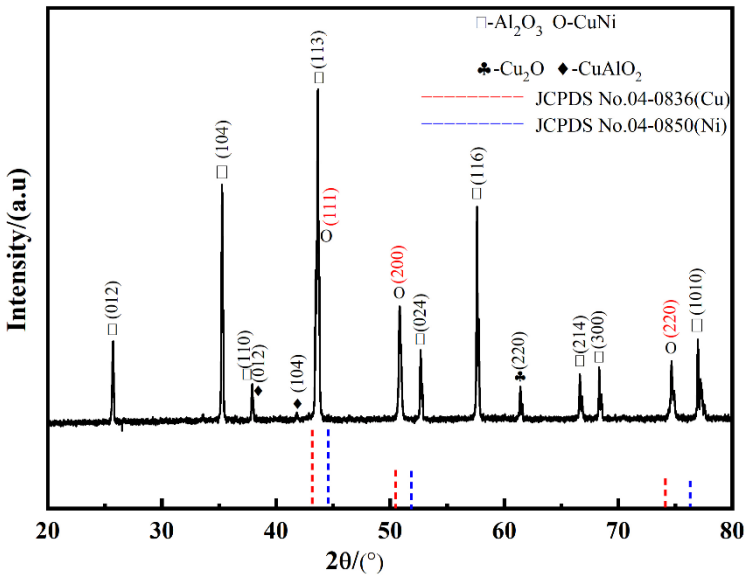

Fig. 5. XRD pattern of Cu/Ni coated Al_2O_3 composite after SPS process.

Composites are composed of two or more different phases. The interfacial bonding strength between different phases has a very important influence on the properties of the composites. The interface acts as a bridge between phases. When the interface bonding is weak, the interface may be separated, forming holes, and cracks when deformed. Therefore, it is necessary to study the interface of composite materials.

Fig. 6 shows TEM image of interfacial structure for the Ni@Al_2O_3/Cu composites. Fig. 6 (a) is the bright field image of the Ni@Al_2O_3/Cu composites. The ellipsoidal substance (marked as 1) is Al_2O_3. The black area surrounding it (marked as 2) is CuNi (a solid solution). The gray white area (marked as 3) between the above two is Cu_2O. Their corresponding selected area electron diffraction (SAED) patterns are shown in Figs. 6(b) to 6(d). The SAED results confirm that during the sintering process Cu atoms are successfully diffused with Ni into the Al_2O_3 surface, and a Cu_2O transition layer is formed on the surface of Al_2O_3 framework. Fig. 6(e) is an inverse Fourier transform (IFT) diagram of HR-TEM image for the solid solution at position 2 in Fig.

6(a). After calibration, it is found that the average spacing between the atomic planes corresponds to the CuNi, which can be confirmed by the XRD results. This proves that Ni atoms have been uniformly diffused into the Cu lattice during sintering. Fig. 6(f) shows the HR-TEM image of the interface position (e.g., position 4 of Fig. 6(a) between Al_2O_3 and Cu_2O. Clearly there is a layer of transition phase of ~5 nm thick between Cu_2O and Al_2O_3, which is $CuAlO_2$ with a hexagonal close-packed (HCP) structure. We can also observe a coherent interface between $CuAlO_2$ (006) plane // Al_2O_3 (006) plane, which indicates that the Al_2O_3-$CuAlO_2$-Cu_2O are closely bonded without apparent mismatching or impurities.

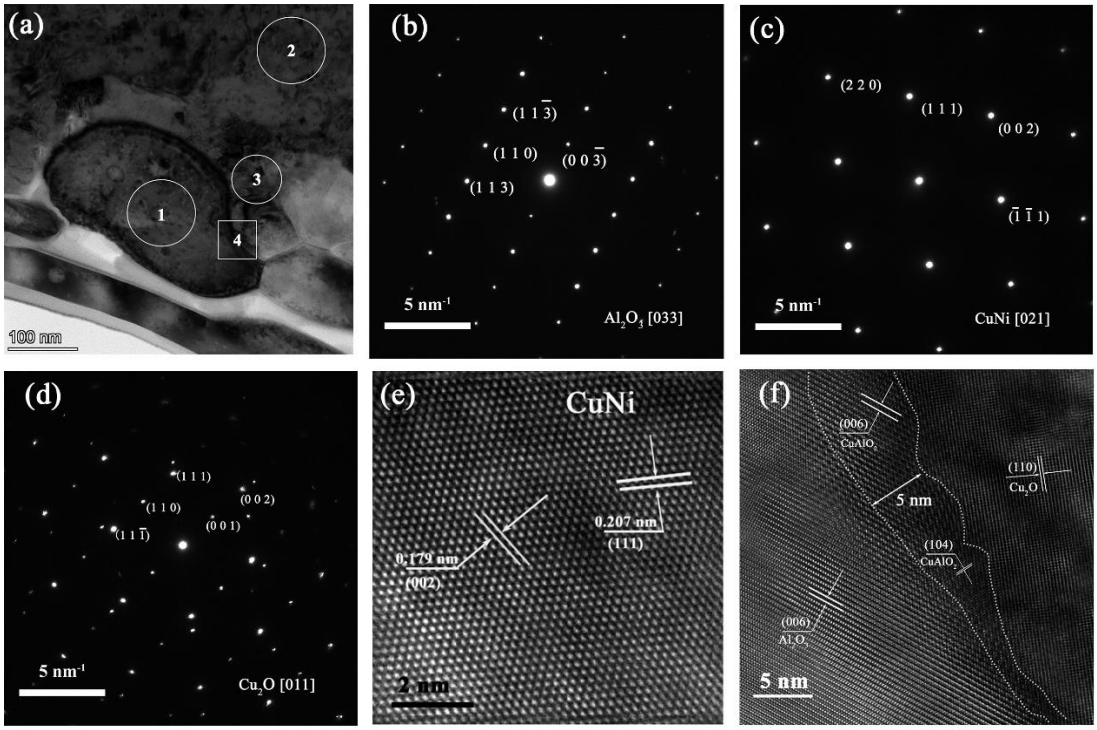

Figu.6. (a) Cu/ Ni@Al_2O_3 TEM diagram of composite interface; (b-d) the SEAD diagram at position 1-3 in figure 6(a); (e) the inverse Fourier transform map corresponding to the HR-TEM diagram at position 2 in figure 6(a) ; (f) the HR-TEM diagram at position 4 in figure6 (a)

Fig. 7 shows XPS spectra of the Ni@Al_2O_3/Cu composite. Fig.7(a) is the survey

spectrum of the sample, which shows that there are Cu, Al, O, C elements in the sample, with weak peak of N. The peak value of Cu 2p for this sample is 932.4 eV. If compared with the standard peak value of Cu (932.7 eV) [30], the binding energy of Cu 2p for this sample was shifted ~0.3 eV. Therefore, the XPS peaks of other elements were adjusted~0.3 eV. Figs.7(b-f) are the high-resolution spectra of Al 2p, O1s, Cu 2p and Ni 2p.

Fig.7(b) shows that the main binding energy peak of Al 2p is 75 eV, which is corresponding to that of Al^{3+} in Al_2O_3. Compared with the binding energy (74.7eV) of Al^{3+} characteristic peak reported in literature [20], it has shifted ~0.3 eV. This is mainly caused by the formation of Al-O-Cu bonds due to the introduction of metallic Cu. Fig. 7(c) shows the O1s spectrum. There is only one characteristic peak, and the corresponding binding energy is 531.4 eV, corresponding to the O in the alumina lattice.

There are two characteristic peaks for the Cu 2p spectrum as shown in Fig.7(d). They correspond to the binding energies of Cu 2p3/2 and Cu 2p1/2, with their binding energies at 932.4 eV and 952.3 eV respectively, corresponding to those of the pure metallic Cu and Cu^+ states [20]. Compared with that of pure metallic Cu, the peak of $Cu2p_{1/2}$ for the $Ni@Al_2O_3/Cu$ is shifted ~0.2–0.4 eV toward higher binding energy. This is mainly due to the formation of CuNi solid solution, so that there is electron transfer between copper and nickel. AES analysis using the Cu LMM spectra can be used to distinguish the Cu^0 and Cu^+ species [20]. The AES measurement result of samples are shown in Fig.7(e). The electron kinetic energy of 914.1 eV is

corresponding to Cu^{+} and the electron kinetic energy of 918.2 eV is corresponding to Cu^{0} [31]. Fig. 7(f) shows the high-resolution Ni 2p spectrum of the Ni@Al_2O_3/Cu composites. The spin-orbit splitting of Ni 2p ($2p_{3/2}$ and $2p_{1/2}$) is dominated by the binding energy located at 853.9 eV and 871.8 eV with a spin–orbit splitting of 17.9 eV, which are corresponding to Ni^{0} state. Compared with the Ni^{0} 2p3/2 of the pure Ni (852.7 eV), the peak of Ni 2p3/2 for Ni@Al_2O_3/Cu composites is shifted ~1.2 eV toward higher binding energy [30]. This indicates that during the sintering process, Ni on the ceramic surface reacts with copper and forms CuNi solid solution, thus causing the electron transfer between copper and nickel.

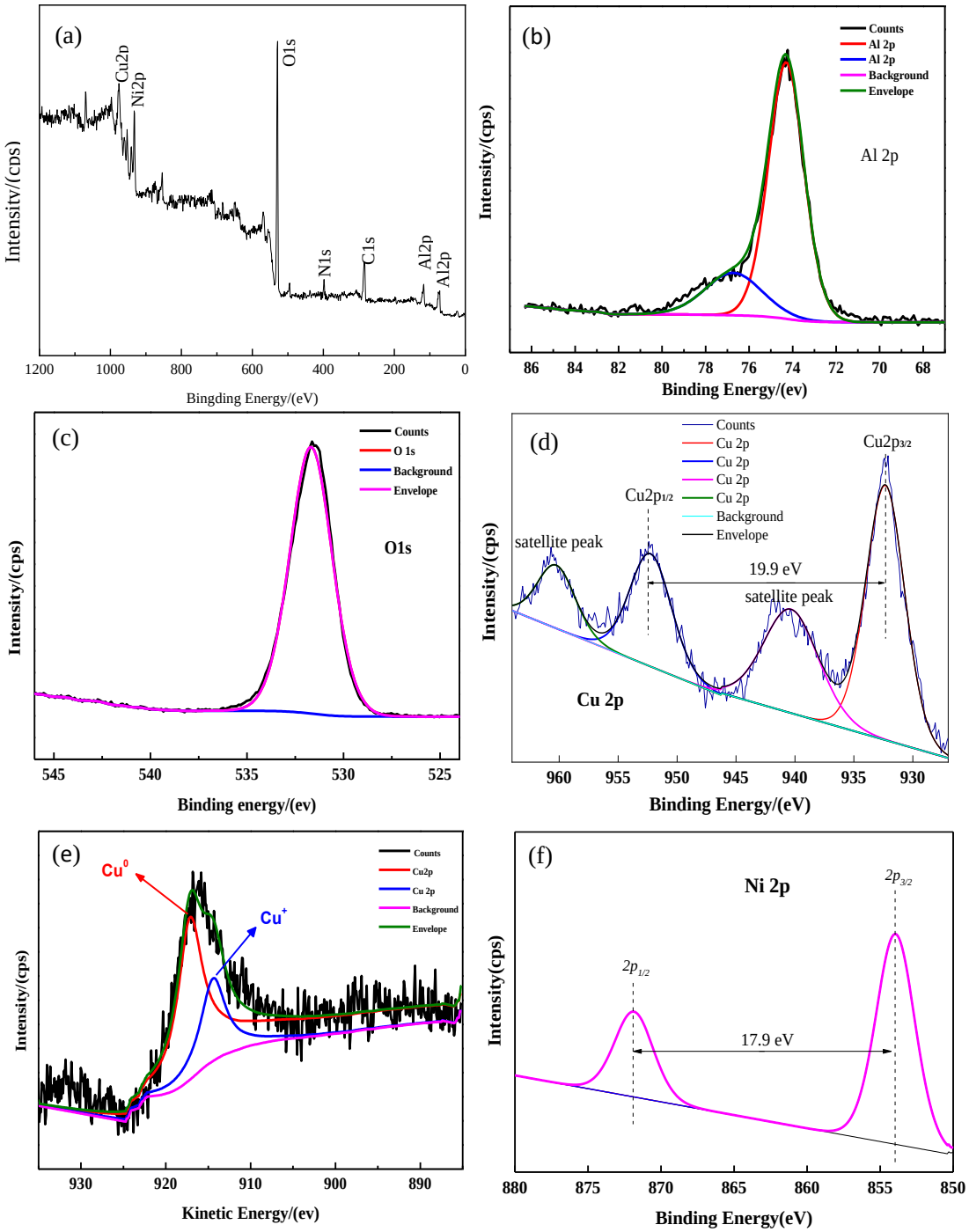

Fig.7. (a) XPS survey spectrum of Ni@Al_2O_3/Cu composite; (b) to (d) high resolution spectra of Al 2p, O 1s and Cu 2p; (e) AES peaks of Cu 2p; (f) XPS high resolution spectra of Ni 2p.

The mechanical properties and electrical properties of the Ni@Al_2O_3/Cu composites prepared using the Ni@Al_2O_3 coated powders after the SPS sintering were characterized, and the results are listed in Table 2. It can be seen that the fracture

toughness and relative density of the composites are significantly higher than the values reported in the literature [15,32,33], indicating that applying a Ni layer has a significant enhancement effect on Ni@Al_2O_3/Cu composites. The resistivity of the Cu/Ni@Al_2O_3(1.28×10^{-3} Ω·m) is much lower than that of Cu/Al_2O_3 (2.0×10^{-3}Ω·m based on our previous work [20]), mainly because the Ni layer promotes the dispersion of the Cu phase in the composites.

Table 2. Mechanical and electrical properties of the Ni@Al_2O_3/Cu composites after the SPS sintering with coated Al_2O_3 powders.

Samples	Sintering	Fracture toughness /(MPa·$m^{1/2}$)	Relative density/(%)	Resistivity/(Ω·m)	Reference
Cu/Al_2O_3(15 vol%) Ni coated powders	SPS	6.72	99.3	$1.28*10^{-3}$	Present work
Cu/Al_2O_3(5 vol%)	HP	5.57	96.2	-	[15]
Cu/Al_2O_3(5 vol%)	HP	4.92	97.6	-	[26]
Cu/Al_2O_3(10 mol%)	HP	5.43	97.4	-	[27]

3.3 Interfacial wettability and strengthening mechanisms of Ni@Al_2O_3/Cu composites

Effect of Ni coating on the wettability of metallic Cu and ceramic phase Al_2O_3 was further studied. Fig. 8(a) shows the wetting angle of the molten Cu on the pure alumina ceramic, and Fig. 8(b) shows that angle on the Ni-coated sample. The wetting angles on two substrates were measured (see the embedded Table in Fig. 8). The wetting angle on the pure alumina surface is 117.3°~125.5°, which is consistent with the data in ref.[10]. Whereas on the Ni@Al_2O_3 surface, the wetting angle is 86.2°~90.5°. Liu et al. [34] reported that Ni coating was deposited on the surface of alumina substrate using a chemical vapor deposition, and the wetting angle of copper droplets on the Ni coated Al_2O_3 was reduced from 128° to 30.15°. From our results, it can also be proved that the Ni layer improves the wettability of the system.

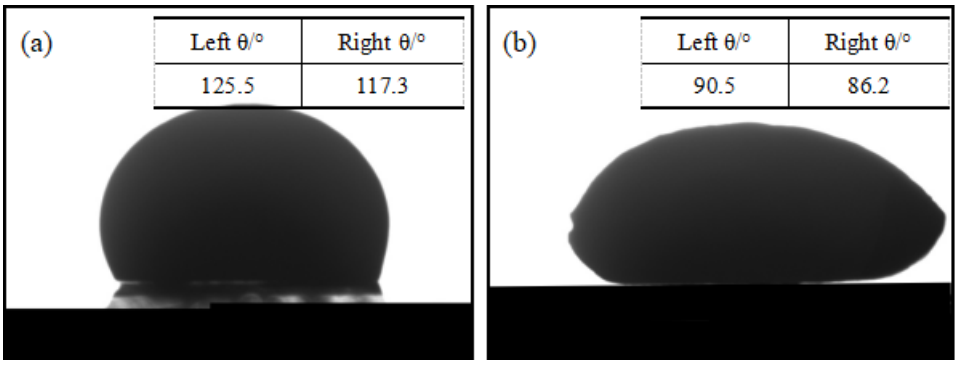

Fig. 8. Optical micrographs of contact angles of a droplet on (a) pure alumina ceramic, (b) Ni-coated alumina measured at room temperature using the droplet method.

According to Young-Dupre's equation:

$$\gamma_{sg} = \gamma_{sl} + \gamma_{gl}\cos\theta \quad (7)$$

$$W_{sl} = \gamma_{gl}(1+\cos\theta) \quad (8)$$

where γ_{sg} is the solid surface energy; γ_{sl} is the solid-liquid interface energy; γ_{gl} is the liquid metal surface energy; θ is the wetting angle; W_{sl} is the solid-liquid adhesion energy per unit area. It can be seen that the wettability between copper and alumina is mainly determined by solid surface energy γ_{sv}, Ni@Al_2O_3/Cu solid-liquid interface energy γ_{sl} and liquid metal Cu surface tension γ_{lv}. Because of the existence of this Ni layer, the bridging connections among Al_2O_3, Ni and Cu are formed between Ni@Al_2O_3/Cu interfaces during the melting of metals, which reduces the surface tension of liquid metal and also the γ_{sl} value of liquid solid interface, thereby effectively reducing the wetting angle and increasing solid-liquid adhesion energy between Ni@Al_2O_3 and molten Cu. In addition, as revealed from both XRD and XPS analysis, Ni promotes the interfacial reactions between Cu and Al_2O_3, and causes the formation of Cu_2O and $CuAlO_2$. The co-existence of Cu_2O and $CuAlO_2$ plays an important role in improving the wettability of the system. Ghetta et al. [35] previously

reported that dissolution of oxygen in the molten Cu decreases the contact angle θ by forming interfacial oxides and the contact angle θ was decreased accordingly.

Based on our characterization results, we can obtain that the following reasons can be attributed to the enhancement in the mechanical properties by adding the Ni layer.

(1) Firstly, the presence of the Ni layer improves the wettability of Cu with the alumina matrix and promotes formation of dense interfacial structures.

(2) Secondly, the presence of Ni layer promotes the diffusion and interfacial reactions between Cu and Al_2O_3 and the formation of the Cu_2O and $CuAlO_2$, which contributes to the improvement of wettability. In addition, the liquid phases penetrate into the skeleton ceramic framework uniformly, which avoids the agglomeration of the metal phase. This will improve the fracture toughness, relative density and electrical conductivity of the composites.

(3) Thirdly, SPS process produces a plasma enhancing effect and locally generates high temperature, and thus a full sintering of the ceramic skeleton structure can be quickly formed to ensure that the composite material with a high hardness. The pressure generated in the process overcomes the surface tension of copper to realize a full densification and disperses the metal uniformly so that the high density and high fracture toughness of the Ni@Al_2O_3/Cu composite material are realized.

Fig. 9 illustrates the enhancement mechanism of using the Ni layer in the process. From Figs. 9(a) and 9(b), Ni is well bonded onto the alumina matrix (e.g., forming Al-O-Ni), and the molten Cu does not directly contact with Al_2O_3, but forms a solid-solution contact with the metallic Ni. Simultaneously the Ni layer effectively

reduces the wetting angle of molten Cu and ceramic skeleton, and promotes the interfacial bonding (e.g., formation of Al-O-NiCu-Cu). As the sintering continues, the diffusion and redistribution of materials occur (as shown in Fig. 9(c)). Al_2O_3 will become dissociated into Al and O atoms. Atoms of oxygen combine with the metallic Cu to form oxides such as CuO and Cu_2O. These oxides subsequently react with the alumina matrix to form $CuAlO_2$ mesophases (as shown in Fig. 9(d)). Ni atoms are continuously diffused into copper. After the SPS, Ni exists in the composite material as a solid solution atom. Based on this mechanism, there are multiple phenomena occurring during the sintering process, including interfacial infiltration, interfacial diffusion and surface diffusion, chemical reactions, chemical bonding and physical adsorption. All of these will promote the interface bonding between the Al_2O_3 ceramic and Cu and improve the mechanical properties of the sintered composites.

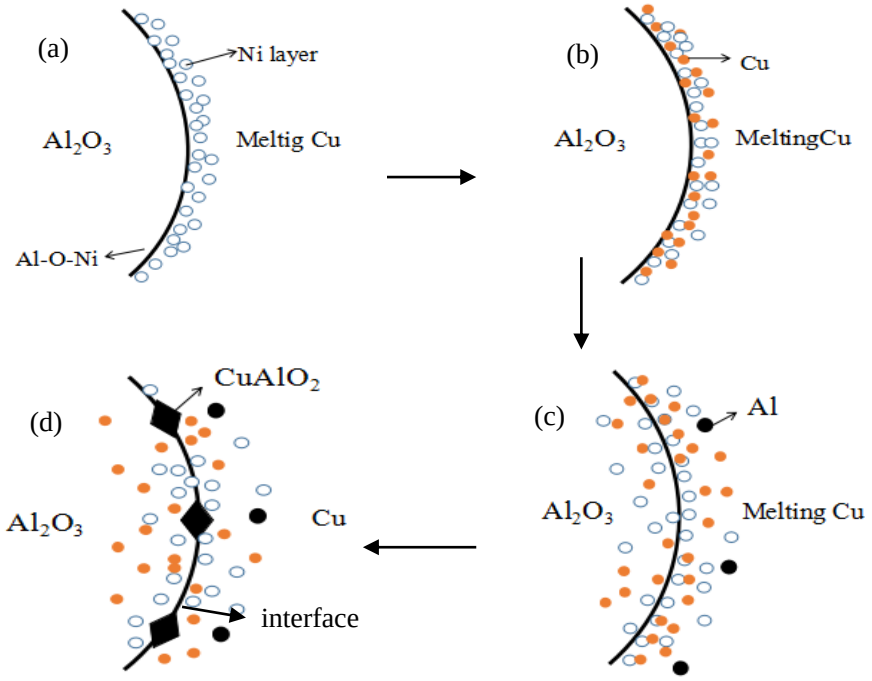

Fig. 9. Illustration of effect of Ni coating on the changes of interfacial structures between Al_2O_3 ceramic and metallic Cu

4. Conclusions

Following conclusions can be obtained from the experimental and analysis results:

1. Ni coated Al_2O_3 composite powders with a uniform network structure were successfully prepared using a heterogeneous precipitation process by optimizing the process parameters. The presence of the Ni layer results in the wetting angle between the ceramic Al_2O_3 and the Cu to be reduced from 128^o to 86.2^o.

2. The ceramic matrix Ni@Al_2O_3/Cu composites with 15 vol% copper content was obtained by SPS sintering using the Ni@Al_2O_3 powders. The microstructure was dense and the phases were evenly distributed. The fracture toughness is 6.72 MPa·m$^{1/2}$, the resistivity is 1.28×10^{-3} Ω·m and the relative density is 99.3%, which are all higher than those reported in literature.

3. The mechanisms of enhancing mechanical properties using the Ni coated powders can be attributed to: (1) well-formed ceramic/metal interfaces which solve the issue of poor wettability of Al_2O_3 with Cu, and thus improve the homogeneous structure; (2) strengthened interfacial bonding between Al_2O_3 and Cu; (3) enhanced material diffusion and interfacial reactions, which result in the formation of Cu_2O and $CuAlO_2$ and improve interfacial wetting properties.

Acknowledgements

The authors would like to acknowledge the financial supports from Xi'an Science Research Project of China (No. 2020KJRC0089) and Shaanxi Coal Industry Group United Fund of China (No.2019JLM-2), and Electrical Materials and Infiltration Key Laboratory of Shaanxi Province, Newton Mobility Grant (IE161019) through

Royal Society and the National Natural Science Foundation of China, and Royal academy of Engineering UK-Research Exchange with China and India.

Conflict of interest

The authors declared that they have no conflicts of interest to this work. We declare that we do not have any commercial or associative interest that represents a conflict of interest in connection with the work submitted.

Reference

[1] Palmero P, Esnouf C, Montanaro L, Fantozzi G (2016) Conventional sintering route for the production of alumina-based nanocomposites: a microstructural characterization. Key Eng. Mater. 318 (15):267–270

[2] Lu H, Hu J, Chen C, Sun H, Hu X, Yang D (2015) Characterization of Al_2O_3-Al nano-composite powder prepared by a wet chemical method. Ceram. Int. 31(3):481–485

[3] Nawa M, Sekino T, Niihara K (1994) Fabrication and mechanical behaviour of Al_2O_3/Mo nanocomposites. J. Mater. Sci. 29:3185–3192

[4] Li G, Huang X, Guo J (2003) Fabrication and mechanical properties of Al_2O_3-Ni composite from two different powder mixtures. Mater. Sci. Eng. A 352:23–28

[5] Rodriguez-Suarez T, Bartolome´ J, Smirnov A, Lopez-Esteban S, D´az L, Torrecillas R, Moya J (2011) Electroconductive alumina-TiC-Ni nanocomposites obtained by spark plasma sintering. Ceram. Int. 37 (5) :1631–1636

[6]Liu Y, Cai X, Sun Z, Jiao X, Akhtar F, Wang J, et al(2018) A novel fabrication strategy for highly porous FeAl/Al_2O_3 composite by thermal explosion in vacuum. Vacuum. 149:225-230

[7]Zhao Y, Zheng Y, Ding W, Zhou W, Zhang G, Liu Z ,et al (2017) Effect of TiO_2 addition on

the densification behavior, microstructure and mechanical properties of Al_2O_3-Cr cermets prepared via vacuum sintering. Vacuum.146:274-277

[8] Lee G, Huang X, Guo J (2001) Improvement of interfacial wettability of Al_2O_3 based. Mater. Rev. 15 (4):33–34

[9] Hanyaloglu S, Aksakal B, McColm I (2001) Reactive sinting of electroless nickle –plated aluminum powders. Mater Charact. 47:9–16

[10] Lee G, Huang X, Guo J (2002) Ni-coated Al_2O_3 powders. Ceram. Int. 28(6):623–626

[11] Huang L,Li J (1999) Properties of cobalt-reinforced Al_2O_3-TiC ceramic matrix composite made via a new processing route.Compos. Pt. A-Appl. Sci. Manuf. 30(5):615–618

[12] Zhang C, Ling G, He J (2003) Co-Al_2O_3 nanocomposites powder prepared by electroless plating. Matter. Letter. 58:200–204

[13] Chen W, Shi Y, Dong L, Li H, Fu Y (2017) Infiltration sintering of WCu alloys from copper-coated tungsten composite powders for superior mechanical properties and arc-ablation resistance. J. Alloy. Compd. 728:196–205.

[14] Nasrabadi H, Sajjadi S, Zebarjad S (2011) Preparation of Al_2O_3/Cu nanocomposite powder by electroless plating and subsequently sintering, Engineering and Medicine-NTC.

[15] Lu H, Sun H, Chen C, Zhang R, Yang D, Hu X (2006) Coating Cu nano-sized particles on Al_2O_3 powders by a wet-chemical method and its mechanical properties after hot press sintering. Mat. Sci. Eng. A-Struct, 426:181–186

[16] Uyasl M，Karslioglu R, Alp A (2013) The preparation of core-shell Al_2O_3/Ni composite powders by electroless platin. Ceram. Int, 39 :5485–5493.

[17] Mazahery A, Shabani M (2012) Influence of the hard coated B_4C particulates on wear

resistance of Al/Cu alloys. Compos. Pt. B-Eng. 43(3):1302–1308

[18] Shi G, Zhang Z, Yang H (2004) Al_2O_3/Fe_2O_3 composite-coated polyhedral Fe nanoparticles prepared by arc discharge. J. Alloy. Compd. 384:0–299

[19] Shen X, Jing M, Li W, Li D (2005) Fabrication of Fe, Ni and FeNicoated Al_2O_3 core-shell microspheres by heterogeneous precipitation. Powder Technol. 160(3):229–233

[20] Shi Y, Chen W, Dong L, Li H, Fu Y (2018) Ehancing copper infiltration into alumina using sparking plasma sintering to achieve high performance Al_2O_3/Cu composites. Ceram. Int, 44: 57–64

[21] G. Greczynski, L. Hultman (2017) C1s peak of adventitious carbon aligns to the vacuum level: dire consequences for material's bonding assignment by photoelectron spectroscopy. ChemPhysChem, 18:1507–1512.

[22] G. Greczynski, L. Hultman (2018) Reliable determination of chemical state in x-ray photoelectron spectroscopy based on sample work function referencing to adventitious carbon: resolving the myth of apparent constant binding energy of the C 1s peak, Appl. Surf. Sci., 451: 99–103.

[23] Somjaijaroen N, Sakdanuphab R, Chanlek N (2019) Simultaneous O_2 plasma and thermal treatment for improved surface conductivity of Cu-Doped SnO_2 films[J]. Vacuum, 166:212–217.

[24] Li G, Dai J (2000) The liquid aluminum in the alumina wetting property improvement. Mater. Eng, 24:11–13

[25] Zhang W, Smith J, Evans (2002) A The connection between ab initio, calculations and interface adhesion measurements on metal/oxide systems: Ni/Al_2O_3, and Cu/Al_2O_3, Acta

Mater.50 (15):3803–3816

[26] Lu P (1996) Science Foundation of Inorganic Materials. Wuhan University of Technology Press, Wuhan, China.

[27] Lan G, Jiang Y, Yi D, Liu S (2013) Theoretical prediction of microstructure evolution during the internal oxidation fabrication of metal-oxide composites: the case of Cu-Al_2O_3. RSC Adv.3(36):16136

[28] Liang S, Fan Z, Xu L, Fang L (2004) Kinetic analysis on Al_2O_3/Cu composite prepared by mechanical activation and internal oxidation. Compos. Pt. A-Appl. Sci. Manuf. 35(12):0–1446

[29] Beraud C, Courbiere M, Esnouf C, Juve D, Treheux D (1989) Study of copper-alumina bonding. J. Mater. Sci. 24:4545–4554

[30] Chen, Y., Yang, Y., Tian, S., Ye, Z., & Li, G. (2019) Highly effective synthesis of dimethyl carbonate over CuNi alloy nanoparticles@porous organic polymers composite. Applied Catalysis A: General, 587, 117275.

[31] Carrasco-Díaz M, Castillejos-López E, Cerpa-Naranjo A, Rojas-Cervantes M (2016) Efficient removal of paracetamol using $LaCu_{1-x}M_xO_3$ (M=Mn, Ti) perovskites as heterogeneous Fenton-like catalysts. Chem. Eng. J. 304:408-418

[32] Oh S, Lee J, Sekino T, Niihara K (2001) Fabrication of Cu dispersed Al_2O_3 nanocomposites using Al_2O_3/CuO and Al_2O_3/Cu-nitrate mixtures. Scripta Mater, 44:2117–2120

[33] Hou T, Han D, Zhang R, Lu H (2008) Study on preparation and properties of Al_2O_3/Cu composites by packaging and hot pressing. Hot Work. Tech. 37:18–21

[34] Liu J, Sang K, Han L (2014) Chemical vapor deposition (CVD) Ni coating on Al_2O_3 ceramic

surface and its wettability with Cu. J. Chin Silic. Soc, 42:397–401

[35] Ghetta V, Fouletier J, Chatain D (1996) Oxygen adsorption isotherms at the surfaces of liquid Cu and Au-Cu alloys and their interfaces with Al_2O_3 detected by wetting experiments. Acta Mater, 44:1927–1936